Ab initio study of magnetic nanopatterning of a hybrid transition metal dichalcogenides/Ir(111) system via magnetic clusters

Vasile Caciuc ⬤,[*] Nicolae Atodiresei,[†] and Stefan Blügel

Peter Grünberg Institut (PGI-1) and Institute for Advanced Simulation (IAS-1), Forschungszentrum Jülich
and JARA, D-52425 Jülich, Germany

In this theoretical study we scrutinized how the interaction between a magnetic cluster made of three Fe atoms and a MoS_2 monolayer adsorbed on Ir(111) reciprocally modifies their structural, electronic, and magnetic properties. From the structural point of view, the sulfur atom directly coordinated by the Fe cluster is pulled out of MoS_2 on Ir(111) while this behavior is not present for a freestanding MoS_2 single layer. Interestingly, this observation implies that Ir(111) catalyzes such a structural change in MoS_2 upon the magnetic cluster adsorption. Besides this, from the magnetic point of view, the sulfur atom lifted from the transition metal dichalcogenide (TMD) monolayer acquires a small magnetic moment and forms together with the Fe atoms a reactive local heterogeneous chalcogene–transition metal magnetic unit that can be employed to functionalize TMD-based hybrid systems.

I. INTRODUCTION

Two-dimensional (2D) materials such as transition metal dichalcogenides (TMDs) [1–4] with the chemical formula MX_2 (*M* is a transition metal from the group IV, V, or VI and *X* is a chalcogen one) have opened new fascinating perspectives on designing low-dimensional electronic devices as shown, for example, by the use of TMD semiconductors in field effect transistors [5], integrated circuits [6], or optoelectronics [7,8].

Regarding the spintronic applications of TMDs, the spin-dependent transport in TMD-based spin-valve devices was experimentally investigated for the nonmagnetic MoS_2 spacer inserted between two NiFe [9] and Fe_3O_4 [10] electrodes. Additionally, the spin injection in WSe_2 from a ferromagnetic contact can be used to generate a valley polarization as revealed by electroluminescence measurements [11].

To gain a fundamental understanding on how to specifically tailor the functionality of TMDs in spintronics [12], several theoretical studies have been dedicated to investigate the electronic and magnetic properties of freestanding TMD monolayers incorporating magnetic 3*d* transition metal (TM) atoms such as vanadium in VS_2, VSe_2, and VTe_2 [13–15] or doped with magnetic and nonmagnetic 3*d* TMs [16–18]. Furthermore, it was also theoretically suggested that a magnetic behavior can be induced in the nonmagnetic ReS_2 single layer by fluorination [19], by strain in the hydrogenated MoS_2 [20] and TaX_2 (*X* = S, Se, and Te) [21] ones, or only by hydrogenation in the PtS_2, $PtSe_2$, and $PtTe_2$ monolayers [22]. Regarding the magnetic TMD monolayers as in the case of VTe_2, a switch between a ferromagnetic and antiferromagnetic state can be obtained by adsorbing H adatoms and by

applying strain [23], or the magnetic features of a $TaTe_2$ single layer can be modified with the help of external strain [24]. Furthermore, the electronic and magnetic fingerprints of the hybrid interfaces formed by TMD single layers on magnetic substrates that are relevant for spin injection have also been theoretically investigated as in the case, for instance, of the MoS_2 monolayer on Gd(0001) [25] and Co(0001) [26] or MoX_2 (*X* = Se, Se, and Te) on Ni(111) [27] (see also Refs. [28,29]).

An alternate route to induce magnetism in TMD-based systems is to consider magnetic clusters adsorbed on TMDs or intercalated between the TMD layers as shown for Mn_n (*n* = 1, 4) clusters on single and bilayer MoS_2 [30]. In particular, reactive magnetic clusters on TMDs can serve as templates for the adsorption of organic molecules that in turn can modify their magnetic properties like the exchange coupling constants due to the formation of hybrid molecule/cluster/surface magnetic units as already shown for organic molecules on magnetic surfaces [31–33].

In this respect, in a previous theoretical investigation we systematically analyzed the structural, electronic, and magnetic properties of hybrid systems consisting of several magnetic and nonmagnetic TMD monolayers on Fe/Ir(111) [34]. Particularly, our first-principles results demonstrated that indeed a magnetic hardening effect for the calculated exchange coupling constants of the Fe surface atoms is present as previously revealed for hybrid molecular–magnetic surface systems [31–33]. On this basis, in this *ab initio* study we explored how the adsorption of a magnetic cluster made of three Fe atoms (Fe_3) on MoS_2/Ir(111) can be employed to reciprocally tailor their electronic and magnetic properties.

More specifically, our first-principles results revealed that the adsorption of the Fe_3 cluster significantly changes the geometry of the MoS_2 deposited on the Ir(111) substrate by pulling out the sulfur atom directly coordinated by the three

---

[*]v.caciuc@fz-juelich.de

[†]n.atodiresei@fz-juelich.de

Fe atoms above them. Notably, this structural change was also obtained in the case of a second Fe_3 cluster on MoS_2/Ir(111). However, the interaction of the Fe_3 cluster with a freestanding MoS_2 single layer does not lead to this behavior even if the configuration with a sulfur atom extracted from surface is the ground-state one. This observation implies that the presence of the Ir(111) plays a crucial role in removing the corresponding energy barrier. Besides this, the sulfur atom pulled out of the MoS_2 surface becomes magnetic with a spin-density distribution similar to the shape of an sp^3 atomic-like orbital directed to the vacuum interface. Therefore, this sulfur atom devises together with the Fe atoms a reactive local heterogeneous chalcogene–transition metal magnetic unit that can serve as a platform to further functionalize such a hybrid system by adsorbing organic molecules as we have already shown, for instance, in the case of iron phthalocyanine (FePc) molecules adsorbed on the silicene/ZrB_2(0001) substrate [35]. More specifically, in that combined experimental and theoretical study we demonstrated that the sp^3-like dangling bonds of the Si atoms at the silicene domain boundary form a chemical bond with the Fe atom of FePc whose sharp electronic states closely resemble those of a freestanding FePc molecule and this molecular patterning remains stable even at room temperature.

II. COMPUTATIONAL SETUP

Our density functional theory (DFT) [36,37] calculations were performed using the projector augmented wave method (PAW) [38] to provide an all-electron description for the valence electrons whose interactions are described by the generalized gradient approximation [39] to the exchange-correlation energy functional as implemented in the VASP code [40–42]. The electronic and magnetic properties of an iron cluster made up of three atoms (Fe_3) with a collinear (ferromagnetic) alignment of their magnetic moments were investigated when adsorbed on a MoS_2/Ir(111) surface modeled by a $2\sqrt{3} \times 2\sqrt{3}$ transition metal dichalcogenide (TMD) surface unit cell on the 4×4 Ir(111) substrate consisting of six atomic layers. In particular, we focused on a magnetic Fe_3 cluster to have a threefold coordination of the S atoms in the upper atomic layer at the vacuum interface as expected for a system with a hexagonal symmetry. To obtain the ground-state geometry, the atomic degrees of freedom of the Fe, TMD, and first Ir surface layer were relaxed without any symmetry constraint until the calculated forces were smaller than 5 meV/Å for a k mesh of $4 \times 4 \times 1$ and a plane wave kinetic energy cutoff of 500 eV. Note that in the case of two Fe_3 clusters on MoS_2/Ir(111) a less tighter criterion of 20 meV/Å for the Hellmann-Feymann forces was employed. Additionally, the effect of the spin-orbit coupling (SOC) on the electronic structure of the hybrid systems considered in our study was also explored (keeping the Fe_3 cluster in a collinear ferromagnetic magnetic configuration).

III. RESULTS

From the structural point of view, the ground-state geometry of the hybrid Fe_3 cluster/MoS_2/Ir(111) system is illustrated in Fig. 1(a). Similarly to the MoS_2 on Fe/Ir(111)

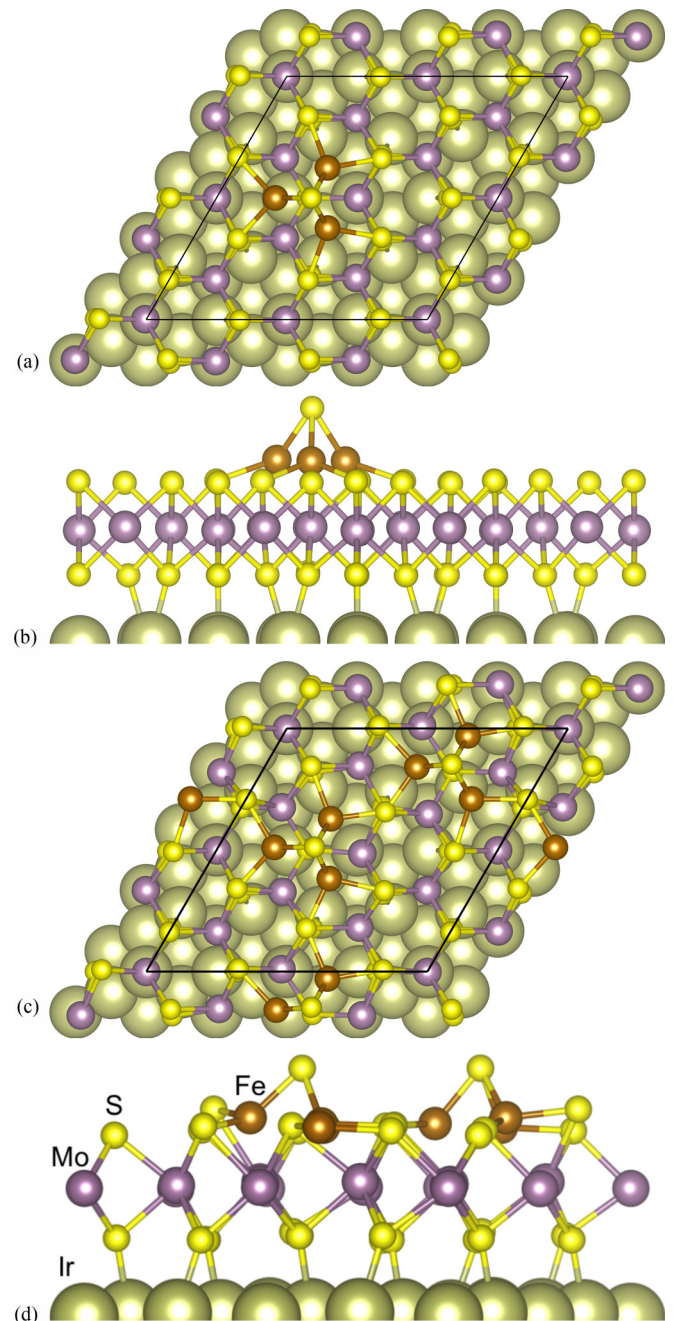FIG. 1. Top (a) and lateral (b) views of the ground-state adsorption geometry for a three-atom Fe cluster adsorbed on $(2\sqrt{3} \times 2\sqrt{3})MoS_2/(4 \times 4)$Ir(111). Interestingly, the lateral view of this structure shows the presence of a sulfur atom relaxed out of the atomic plane of the Fe cluster [hereafter denoted as S_{out} and the resulting configuration is referred to as $S_{out}/Fe_3/MoS_2/Ir(111)$]. It is important to mention that this behavior was also observed when a second Fe_3 cluster was deposited on substrate as shown in (c) and (d). These figures were obtained using VESTA [43].

investigated in Ref. [34], on Ir(111) the MoS_2 single layer also has its S atoms in an atop configuration with respect to the Ir atoms in the first metal surface layer such that the sulfur atoms in the lower atomic layer form a chemical bond with the surface Ir atoms as depicted in Fig. 1(b) ($d_{S-Ir} \sim 2.4$ Å). On the other hand, the three-atom Fe cluster adopts an

adsorption geometry with a S atom of the upper atomic layer in its center while the Fe atoms are in atop-top positions with regard to the surface Ir atoms. Interestingly, in this adsorption configuration the S atom in the center of the Fe_3 cluster (denoted hereafter as S_{out}) is pulled out from the upper S atomic plane as shown in Fig. 1(b). It is important to mention that a similar behavior was observed when a second Fe_3 cluster was adsorbed in a similar geometry [see Figs. 1(c) and 1(d)]. Since S_{out} becomes magnetic with a magnetic moment of $0.16\mu_B$ (see below), overall this structural change of the MoS_2 monolayer upon the adsorption of the Fe_3 clusters suggests the possibility of creating a new type of magnetic nanopattern based on magnetic $3d$ and (initially) nonmagnetic $3p$ elements.

It is also important to note that in the case of the same adsorption configuration of the Fe_3 cluster on the freestanding MoS_2 monolayer, the sulfur S_{out} atom was not extracted from the upper S layer. Nevertheless, when slightly shifted by hand above the magnetic cluster, the relaxed geometry of the Fe_3/TMD system is similar to that obtained when the Ir(111) substrate is included; i.e., the S_{out} is also pulled out of the MoS_2 and has a magnetic moment of $\sim 0.18\mu_B$. Interestingly, this S_{out}/Fe_3/MoS_2 configuration is also lower in energy by ~ 4.1 eV than the initial Fe_3/MoS_2 one.

Notably, this observation implies that the presence of the Ir(111) surface removes the energy barrier between these two configurations of the freestanding TMD single layer such that in the case of the hybrid Fe_3/MoS_2/Ir(111) system the S_{out} atom can be lifted from surface leading to the S_{out}/Fe_3/MoS_2/Ir(111) ground-state geometry. In particular, this behavior can be correlated with the fact that the work function of 4.81 eV calculated for the hybrid MoS_2/Ir(111) system is smaller than that of ~ 5.07 evaluated for the freestanding MoS_2 monolayer [44]. Similarly to the case of organic molecules like benzene adsorbed on surfaces with different work functions [45], this implies that on Ir(111) the MoS_2 single layer is more reactive than in the freestanding case. Overall, the increased reactivity of MoS_2 on Ir(111) opens the way to pull out a sulfur atom in the presence of an iron cluster that is also reactive.

From the energetic point of view, the significant local structural change of MoS_2 on Ir(111) upon the adsorption of the three-atom Fe cluster can be associated with the chemisorption bonding mechanism of the Fe atoms on this substrate. Indeed, as indicated in Table I, the calculated adsorption energy of ~ -3.62 eV per Fe atom is clear evidence for a strong chemisorption of the magnetic cluster. Importantly, this adsorption energy is significantly larger than that of ~ -2.11 eV (per Fe atom) evaluated for the Fe_3 cluster on the freestanding MoS_2 single layer, which is directly reflected by a *decrease* of the average Fe-Fe interatomic distance from 2.94 Å for the magnetic cluster on MoS_2 to 2.35 Å when adsorbed on MoS_2/Ir(111). These observations are also clear evidence that MoS_2 on Ir(111) is more reactive than when it is freestanding.

Regarding the electronic structure of the Fe_3/MoS_2/Ir(111) system, the analysis of the spin-polarized projected density of states (SP-PDOS) shown in Fig. 2 indicates a spin-dependent hybridization between the p

TABLE I. The adsorption energy per Fe atom evaluated for the Fe_3 cluster adsorbed on MoS_2/Ir(111) [i.e., for the S_{out}/Fe_3/MoS_2/Ir(111) ground-state configuration], the calculated exchange coupling constant J describing the magnetic interactions between the cluster Fe atoms on MoS_2/Ir(111), and the magnetocrystalline anisotropy energy (MAE) obtained for the ground-state geometry of the hybrid system. As a reference, these physical quantities were also evaluated for the Fe_3 cluster on the freestanding MoS_2 single layer. Interestingly, the MAE evaluated for S_{out}/Fe_3/MoS_2/Ir(111) is slightly smaller than its value obtained for Fe_3/MoS_2 due to a stronger chemisorption in the former case.

System	$E_{ads}^{\text{Fe atom}}$ (eV)	J (meV)	MAE (meV)		
			[100]	[010]	[001]
S_{out}/Fe_3/MoS_2/Ir(111)	-3.624	112.0	1.2	1.2	0.0
Fe_3/MoS_2	-2.109	116.2	1.6	1.6	0.0

state of S_{out} and the d ones of the Fe cluster atoms. In particular, this spin-imbalanced hybridization results in the formation of hybrid cluster/MoS_2/surface states that at S_{out} have an sp^3-like character as illustrated by the plot of the spin polarization depicted in Fig. 3 (see below). Consequently, S_{out} becomes magnetic and acquires a magnetic moment of $\sim 0.16\mu_B$ that is ferromagnetically coupled to the Fe ones ($\sim 2.66\mu_B$) resulting in the formation of a chalcogene–transition metal magnetic cluster. Interestingly, spin-dependent features can also be observed in the SP-PDOS calculated for the Mo atomic layer [see Fig. 2(c)]. More specifically, small magnetic moments are induced also in some of these atoms, especially in those close to the Fe atoms with the largest magnitude of $\sim 0.11\mu_B$.

The presence of a small magnetic moment for the sulfur S_{out} atom can be directly visualized in the real space by plotting the spin-polarization density as shown in Fig. 3(a). Indeed, a positive spin density is piled up at S_{out} that is ferromagnetically coupled to the spin density present at the three Fe atoms. Interestingly, as depicted in Fig. 3(b), this spin accumulation at S_{out} mainly originates from the depletion of the spin density around the Fe_3 cluster atoms.

An additional insight into the spin texture of the hybrid S_{out}/Fe_3/MoS_2/Ir(111) and MoS_2/Ir(111) systems was gained by calculating their band structures including the spin-orbit coupling (SOC) (see Fig. 4). In the case of MoS_2/Ir(111) [see Fig. 4(a)], for the MoS_2 monolayer a fingerprint feature of its band structure induced by the SOC is the inversion of the spin polarization along the $\overline{\Gamma}$-$\overline{K'}$-$\overline{K}$-$\overline{\Gamma}$ direction of the $(2\sqrt{3} \times 2\sqrt{3})$ supercell's Brillouin zone when passing through the $\overline{M}$ high-symmetry k point as in the case of a (1×1) freestanding MoS_2 layer [see also the zoom-in shown in Fig. 4(c)]. However, in contrast to the freestanding MoS_2 layer, generally along the $\overline{\Gamma}$-$\overline{K}$-$\overline{M}$ direction the MoS_2/Ir(111) electronic states have a spin-up or spin-down polarization with different weights at each k point that are then mirrored in states with opposite spin polarization along the $\overline{M}$-$\overline{K'}$-$\overline{\Gamma}$ one. This feature is a direct consequence of the hybridization between the MoS_2 and Ir(111) electronic states. In the case of the S_{out}/Fe_3/MoS_2/Ir(111) system, additionally to the MoS_2-Ir(111) hybridization process, we note that the effect
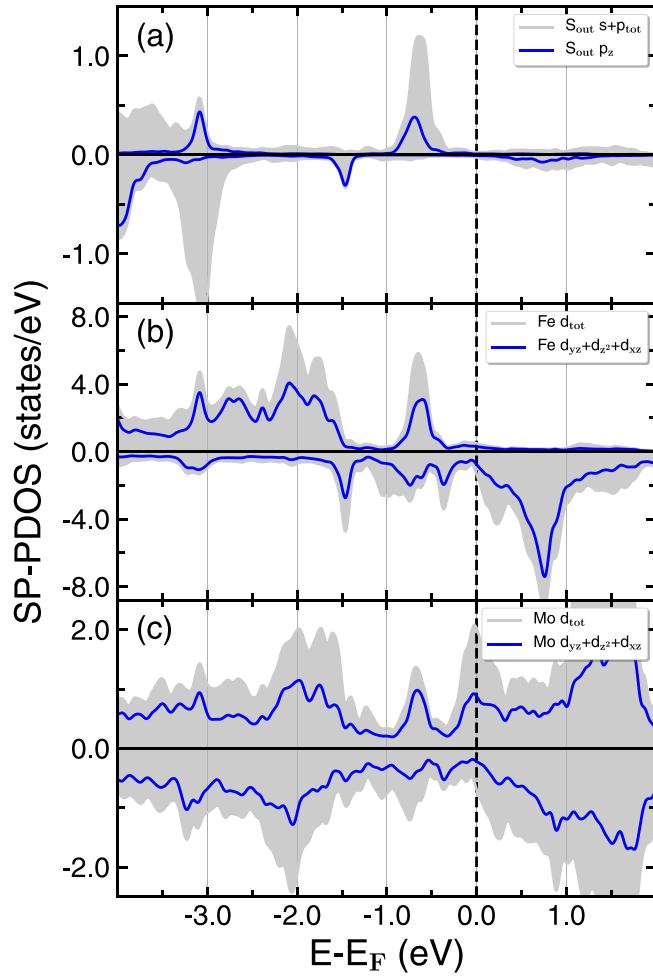
FIG. 2. (a) The spin-polarized atom-projected density of states (SP-PDOS) for the electronic states of the sulfur S_{out} atom pulled out of the TMD surface by its interaction with the Fe_3 cluster and (b) the corresponding total and out-of-plane $(d_{yz} + d_{z^2} + d_{xz})$ d states of the Fe atoms as well as (c) of their three nearest-neighbor Mo atoms. It is important to note the hybridization between the sp^3 atomic-like hybrid orbitals of S_{out} with the d states of the Fe atoms. This observation is in particular apparent for the electronic states in an energy range of $[E_F - 1.0 \text{ eV}, E_F]$. Moreover, the spin-dependent interaction between the Fe and their three neighboring Mo atoms induces spin-polarized features in the electronic structure of these Mo atoms.
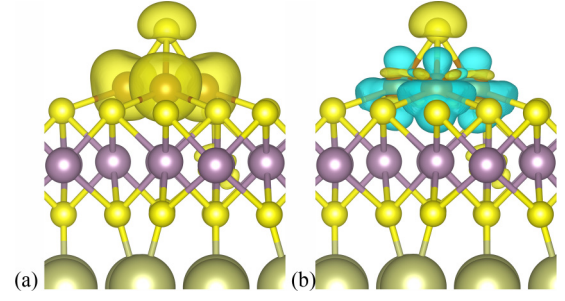
FIG. 3. Lateral views of the real-space distribution (a) of the spin polarization density and (b) the spin polarization density difference plotted for the Fe cluster/MoS_2/Ir(111) system (isosurface of 0.038 electrons/$\mathring{A}^3$). Note that the spin polarization density $\rho_{polariz} = \rho^\uparrow - \rho^\downarrow$ is defined as the difference between the spin-up ($\rho^\uparrow$) and spin-down ($\rho^\downarrow$) densities while the spin polarization density difference is defined as $\Delta\rho_{polariz} = \rho_{polariz}^{system} - \rho_{polariz}^{S_{out}/MoS_2/Ir(111)} - \rho_{polariz}^{Fe_3}$, i.e., the difference between the spin polarization of the hybrid $S_{out}/Fe_3/MoS_2$/Ir(111) system and those of the S_{out}/MoS_2/Ir(111) and Fe_3 cluster with their geometry as in the hybrid system. As a general feature, note the presence of a positive spin density at the sulfur S_{out} atom coupled ferromagnetically to the three Fe atoms. Interestingly, this feature at S_{out} arises from the depletion of the spin density around the cluster Fe atoms and corresponds to a reduction of the magnetic moment from $\sim 3\mu_B$ for the freestanding Fe_3 cluster to $2.66\mu_B$ (per Fe atom) in the case of the hybrid system. The positive spin density is colored in yellow and the negative one in blue.

of the SOC on the hybrid spin-split electronic states that result from the interaction of the MoS_2/Ir(111) with the Fe magnetic cluster is to increase the magnitude of the positive spin polarization in the MoS_2 layer at $\overline{K'}$ and decrease it at $\overline{K}$ for the states near the Fermi energy as clearly illustrated by the zoom-in shown in Fig. 4(d). In practice, these electronic structure features can be explored via spin-polarized angle-resolved photoelectron spectroscopy (SP-ARPES) experiments. Furthermore, from the theoretical point of view an important issue is to investigate in future studies how to tune this feature of the SOC band structure, for instance, by decoupling $S_{out}/Fe_3/MoS_2$ from Ir(111) by inserting semiconductor or insulator spacers [46].

Additionally, one can also notice that the magnetic properties of the Fe_3 cluster on the MoS_2/Ir(111) substrate are not significantly modified as compared to the case when it is on the freestanding MoS_2 layer. More specifically, using a Heisenberg Hamiltonian $H = -\sum_{i>j} J_{ij} \mu_i \mu_j$ that describes the exchange interaction between the nearest-neighbor pairs of atoms i and j with the magnetic moments μ_i and μ_j, the calculated Fe-Fe exchange coupling constant J [47] for the $S_{out}/Fe_3/MoS_2$/Ir(111) system (112 meV) is only slightly smaller ($\sim 4\%$) than that of 116.2 meV evaluated for Fe_3/MoS_2. Nevertheless, it is still ~ 6 times larger than the exchange coupling constant of 18.0 meV calculated for one monolayer of Fe on Ir(111) [48]. Moreover, the magnetocrystalline anisotropy energy (MAE) obtained for $S_{out}/Fe_3/MoS_2$/Ir(111) is slightly smaller than that evaluated for Fe_3/MoS_2 due to a stronger chemisorption and in both cases the easy axis is out-of-plane (see Table I). In particular, it is also important to point out that its value of ~ 1.2 meV is significantly larger than that calculated for the bulk bcc Fe ($\sim 1.1\mu$eV). Generally, this result is similar to those obtained for several π organic molecules adsorbed on magnetic substrates where an increase of MAE (with respect to bulk and clean surfaces) leads to the formation of molecular-based magnetic units that exhibit a magnetic hysteresis as experimentally shown in Ref. [49] and theoretically explored in Ref. [31]. Therefore, a similar behavior is expected in the case of our system; i.e., for $S_{out}/Fe_3/MoS_2$/Ir(111) the interplay between the MAE and a large exchange coupling constant J will stabilize the magnetic properties of the local S_{out}/Fe_3 magnetic unit. Overall, our first-principles results re-
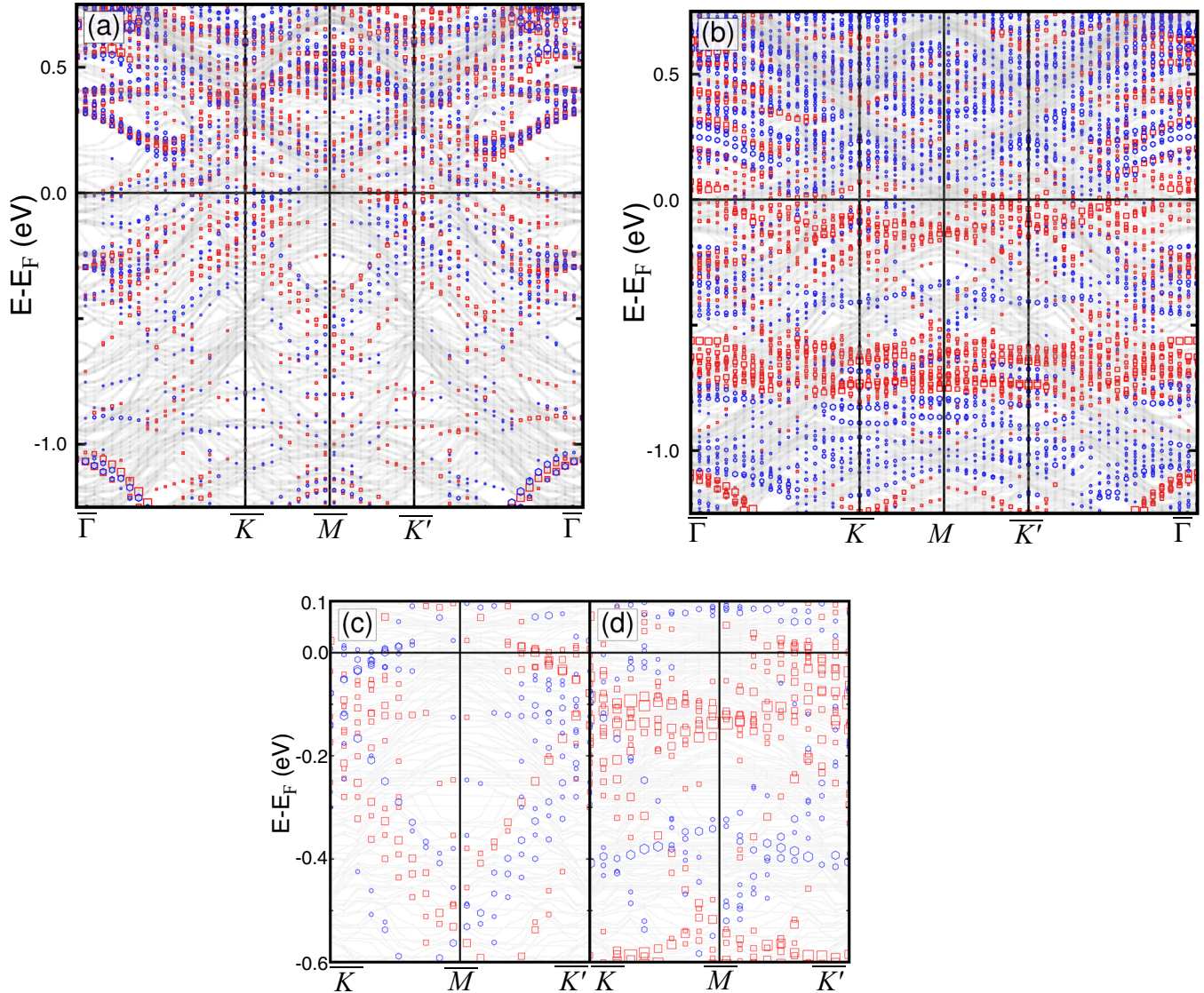
FIG. 4. The band structures calculated for (a), (c) $MoS_2/Ir(111)$ and (b), (d) $S_{out}/Fe_3/MoS_2/Ir(111)$ including the spin-orbit coupling (SOC). The positive and negative spin polarization is indicated by red and blue symbols, respectively, for values larger than 2% when the spin polarization is summed over all atoms in the MoS_2 layer (the size of the symbols is proportional to the degree of spin polarization). In the case of $MoS_2/Ir(111)$ it is worthwhile to recall that the spin polarization of the MoS_2 layer becomes inverted along the $\overline{\Gamma}$-$\overline{K'}$-$\overline{K}$-$\overline{\Gamma}$ direction when crossing through the $\overline{M}$ high-symmetry k point as in the case of the freestanding (1×1) MoS_2 monolayer due to the time-reversal symmetry. However, in contrast to the freestanding MoS_2 monolayer, the hybridization between the MoS_2 and $Ir(111)$ electronic states leads to SOC bands characterized by a spin-up or spin-down polarization with in general different weights at each k point [see the zoom-in shown in (c)]. Besides this, as clearly depicted in (d), the interaction of the Fe_3 magnetic cluster with the $MoS_2/Ir(111)$ substrate increases the magnitude of the positive spin polarization in the MoS_2 layer at $\overline{K'}$ and decreases it at $\overline{K}$ for the electronic states near the Fermi energy.

vealed that the adsorption of an Fe_3 cluster on $MoS_2/Ir(111)$ results in the formation of a heterogeneous chalcogene-Fe cluster with a reactive magnetic S_{out} bonded to three Fe atoms.

IV. SUMMARY AND OUTLOOK

In this *ab initio* study we investigated the structural, electronic, and magnetic properties of a hybrid system obtained by depositing an Fe_3 cluster containing three atoms on the $MoS_2/Ir(111)$ substrate. Interestingly, the interaction of the

Fe_3 cluster with the MoS_2 monolayer significantly changed its geometry in the presence of the $Ir(111)$ surface while this behavior was not observed in the case of the freestanding TMD single layer, which emphasizes the importance of including a real substrate for TMDs in such a study. More specifically, the sulfur atom directly coordinated by the Fe atoms was pulled out of the 2D material above the Fe_3 cluster and acquires a magnetic moment whose distribution in space resembles the shape of an sp^3 atomic-like orbital pointing to the vacuum interface. In consequence, this reactive sulfur atom forms together with the Fe atoms a heterogeneous chalcogene–

transition metal magnetic cluster and therefore this process opens a new way to create a magnetic nanopattern for TMDs in a way similar to the one we have already shown for the sp^3-like dangling bonds of the Si atoms at the silicene domain boundary that pin the FePc molecules in a molecular pattern stable even at room temperature [35]. Therefore, such a local chalcogene-TM magnetic unit can be used, for instance, to further functionalize a hybrid cluster/TMD/substrate system with the help of magnetic and nonmagnetic organic molecules.

[1] Q. H. Wang, K. Kalantar-Zadeh, A. Kis, J. N. Coleman, and M. S. Strano, Nat. Nanotechnol. **7**, 699 (2012).

[2] M. Chhowalla, H. S. Shin, G. Eda, L.-J. Li, K. P. Loh, and H. Zhang, Nat. Chem. **5**, 263 (2013).

[3] X. Xu, W. Yao, D. Xiao, and T. F. Heinz, Nat. Phys. **10**, 343 (2014).

[4] G. Fiori, F. Bonaccorso, G. Iannaccone, T. Palacios, D. Neumaier, A. Seabaugh, S. K. Banerjee, and L. Colombo, Nat. Nanotechnol. **9**, 768 (2014).

[5] B. Radisavljevic, A. Radenovic, J. Brivio, V. Giacometti, and A. Kis, Nat. Nanotechnol. **6**, 147 (2011).

[6] H. Wang, L. Yu, Y.-H. Lee, Y. Shi, A. Hsu, M. L. Chin, L.-J. Li, M. Dubey, J. Kong, and T. Palacios, Nano Lett. **12**, 4674 (2012).

[7] B. W. H. Baugher, H. O. H. Churchill, Y. Yang, and P. Jarillo-Herrero, Nat. Nanotechnol. **9**, 262 (2014).

[8] J. S. Ross, P. Klement, A. M. Jones, N. J. Ghimire, J. Yan, D. G. Mandrus, T. Taniguchi, K. Watanabe, K. Kitamura, W. Yao, D. H. Cobden, and X. Xu, Nat. Nanotechnol. **9**, 268 (2014).

[9] W. Wang, A. Narayan, L. Tang, K. Dolui, Y. Liu, X. Yuan, Y. Jin, Y. Wu, I. Rungger, S. Sanvito, and F. Xiu, Nano Lett. **15**, 5261 (2015).

[10] H.-C. Wu, C. O. Coileái, M. Abid, O. Mauit, A. Syrlybekov, A. Khalid, H. Xu, R. Gatensby, J. J. Wang, H. Liu, L. Yang, G. S. Duesberg, H.-Z. Zhang, M. Abid, and I. V. Shvets, Sci. Rep. **5**, 15984 (2015).

[11] O. L. Sanchez, D. Ovchinnikov, S. Misra, A. Allain, and A. Kis, Nano Lett. **16**, 5792 (2016).

[12] I. Žutić, J. Fabian, and S. D. Sarma, Rev. Mod. Phys. **76**, 323 (2004).

[13] A. Kuc, N. Zibouche, and T. Heine, Phys. Rev. B **83**, 245213 (2011).

[14] Z. Y. Zhu, Y. C. Cheng, and U. Schwingenschlögl, Phys. Rev. B **84**, 153402 (2011).

[15] H.-R. Fuh, C.-R. Chang, Y.-K. Wang, R. F. L. Evans, R. W. Chantrell, and H.-T. Jeng, Sci. Rep. **6**, 32625 (2016).

[16] Y. Zhou, Q. Su, Z. Wang, H. Deng, and X. Zu, Phys. Chem. Chem. Phys **15**, 18464 (2013).

[17] Y. C. Cheng, Q. Y. Zhang, and U. Schwingenschlögl, Phys. Rev. B **89**, 155429 (2014).

[18] A. N. Andriotis and M. Menon, Phys. Rev. B **90**, 125304 (2014).

[19] G. C. Loh and R. Pandey, Phys. Chem. Chem. Phys. **17**, 18843 (2015).

[20] H. Shi, H. Pan, Y.-W. Zhang, and B. I. Yakobson, Phys. Rev. B **88**, 205305 (2013).

[21] P. Manchanda, V. Sharma, H. Yu, D. J. Sellmyer, and R. Skomski, Appl. Phys. Lett. **107**, 032402 (2015).

[22] P. Manchanda, A. Enders, D. J. Sellmyer, and R. Skomski, Phys. Rev. B **94**, 104426 (2016).

[23] H. Pan, Sci. Rep. **4**, 7524 (2014).

[24] H. Guo, N. Lu, L. Wang, X. Wu, and X. C. Zeng, J. Phys. Chem. C **118**, 7242 (2014).

[25] X. Zhang, W. Mi, X. Wang, Y. Cheng, and U. Schwingenschlögl, Sci. Rep. **4**, 7368 (2014).

[26] T. Garandel, R. Arras, X. Marie, P. Renucci, and L. Calmels, Phys. Rev. B **95**, 075402 (2017).

[27] K.-A. Min, J. Cha, K. Cho, and S. Hong, 2D Mater. **4**, 024006 (2017).

[28] M. Y. Yin, X. C. Wang, W. B. Mi, and B. H. Yang, Comput. Mater. Sci. **99**, 326 (2015).

[29] C. Song, S. Gong, Z. Zhang, H. Mao, Q. Zhao, J. Wang, and H. Xing, J. Phys. D: Appl. Phys. **48**, 485001 (2015).

[30] M. Zhang, Z. Huang, X. Wang, H. Zhang, T. Li, Z. Wu, Y. Luo, and W. Cao, Sci. Rep. **6**, 19504 (2016).

[31] M. Callsen, V. Caciuc, N. Kiselev, N. Atodiresei, and S. Blügel, Phys. Rev. Lett. **111**, 106805 (2013).

[32] R. Friedrich, V. Caciuc, N. S. Kiselev, N. Atodiresei, and S. Blügel, Phys. Rev. B **91**, 115432 (2015).

[33] R. Friedrich, V. Caciuc, N. Atodiresei, and S. Blügel, Phys. Rev. B **92**, 195407 (2015).

[34] V. Caciuc, N. Atodiresei, and S. Blügel, Phys. Rev. Mater. **2**, 084001 (2018).

[35] B. Warner, T. G. Gill, V. Caciuc, N. Atodiresei, A. Fleurence, Y. Yoshida, Y. Hasegawa, S. Blügel, Y. Yamada-Takamura, and C. F. Hirjibehedin, Adv. Mater. **29**, 1703929 (2017).

[36] P. Hohenberg and W. Kohn, Phys. Rev. **136**, B864 (1964).

[37] W. Kohn and L. J. Sham, Phys. Rev. **140**, A1133 (1965).

[38] P. E. Blöchl, Phys. Rev. B **50**, 17953 (1994).

[39] J. P. Perdew, K. Burke, and M. Ernzerhof, Phys. Rev. Lett. **77**, 3865 (1996).

[40] G. Kresse and J. Hafner, Phys. Rev. B **47**, 558 (1993).

[41] G. Kresse and J. Furthmüller, Phys. Rev. B **54**, 11169 (1996).

[42] G. Kresse and D. Joubert, Phys. Rev. B **59**, 1758 (1999).

[43] K. Momma and F. Izumi, J. Appl. Cryst. **44**, 1272 (2011).

[44] C. Zhang, C. Gong, Y. Nie, K.-A. Min, C. Liang, Y. J. Oh, H. Zhang, W. Wang, S. Hong, L. Colombo, R. M. Wallace, and K. Cho, 2D Mater. **4**, 015026 (2017).

[45] R. J. Maurer, V. G. Ruiz, J. Camarillo-Cisneros, W. Liu, N. Ferri, K. Reuter, and A. Tkatchenko, Prog. Surf. Sci. **91**, 72 (2016).

[46] H. Schmidt, F. Giustiniano, and G. Eda, Chem. Soc. Rev. **44**, 7715 (2015).

[47] As in Ref. [15] and Refs. [32–34], using this Heisenberg Hamiltonian the Fe-Fe exchange coupling constant J was eval- uated from the total energy difference between the ground-state ferromagnetic magnetic configuration and an antiferromagnetic one.

[48] J. Brede, N. Atodiresei, V. Caciuc, M. Bazarnik, A. Al-Zubi, S. Blügel, and R. Wiesendanger, Nat. Nanotechnol. **9**, 1018 (2014).

[49] K. V. Raman, A. M. Kamerbeek, A. Mukherjee, N. Atodiresei, T. K. Sen, P. Lazić, V. Caciuc, R. Michel, D. Stalke, S. K. Mandal, S. Blügel, M. Münzenberg, and J. S. Moodera, Nature (London) **493**, 509 (2013).